Herschel Oxygen Project

Data Release Document

1. Description of the project and its goals

Molecular oxygen (O_2) is a simple diatomic molecule formed from the third-most abundant element in the universe. The formation of O_2 by gas-phase reactions in the interstellar medium has been studied for many years, and the predicted abundance relative to molecular hydrogen is expected to be ~ 10^{-5}, making molecular oxygen one of the most abundant species in dense molecular clouds (for references to chemistry and other material, see Goldsmith et al. 2011). Molecular oxygen cannot be observed from the ground due to absorption by this species in the Earth's atmosphere. Searches for the $^{16}O^{18}O$ isotopologue, which can be observed from the surface of the Earth, have been carried out. Two space missions, SWAS and Odin, had searches for molecular oxygen as one of their major goals. SWAS did not detect O_2, while Odin made one marginal detection; the general import of both of these missions was that the abundance of molecular oxygen is orders of magnitude below the predictions of gas-phase chemistry.

A number of models to explain this "O_2 deficit" had been developed, based on complex cloud structure involving mass circulation or diffusion, and exposure to UV radiation. Development of models continued as the relatively low abundance of gas-phase water observed by SWAS also suggested a problem with standard chemical models. One of the new features was the recognition that in the colder central regions of clouds, atomic oxygen might stick to dust grains, depriving the gas phase of the key ingredient for making O_2. An essential point was that the grain-surface oxygen would be hydrogenated to water ice, which would remain on the grain surface as long as $T_{grain} \leq 100$ K.

The key goal of the Herschel Oxygen Project (HOP) was to probe a range of molecular cloud environments to detect O_2 or else to obtain better upper limits on its abundance that would help to improve the models of interstellar chemistry. The first key ingredient was the far greater sensitivity of Herschel (HIFI noise temperature ~ 20 times lower than that of SWAS, for example). The second ingredient was the much smaller beam size (up to an order of magnitude smaller than that of SWAS), which would allow probing much more selectively the different regions of molecular clouds, notably the regions in which dust would be sufficiently warm to desorb grain surface ice, either by embedded or external young stars.

2. Anticipated O_2 transitions and HOP data from HIFI

The Heterodyne Instrument for the Far Infrared (HIFI) was selected, as it covers the O_2 transitions expected to be strongest at the temperatures of interstellar clouds, and offers the high spectral resolution necessary to resolve the kinematic structure expected. The lower rotational energy levels and transitions of molecular oxygen are shown in Figure 1. We selected the three strongest O_2 transitions in the range covered by HIFI from energy levels < 120 K above the ground state. Information about these transitions is given in Table 1.

The selection of which transitions to observed was dictated largely by knowledge of the temperature of the source. In addition, the noise temperature of the HIFI receivers increases with increasing frequency, with the result that all sources were observed in the 487 GHz line, but only the warmer sources in the higher transitions. This selection was heavily influenced by the knowledge that the O_2 lines would be relatively weak, and that long integration times would be required. On the other hand, we felt it important that we confirm any detection by observation of more than a single transition wherever possible.

Table 1

Transition (N,J) –(N',J')	Frequency (GHz)	A-coefficient (s^{-1})
3,3 – 1,2	497.249	8.5×10^{-9}
5,4 – 3,4	773.840	4.4×10^{-8}
7,6 – 5,6	1120.715	6.3×10^{-8}

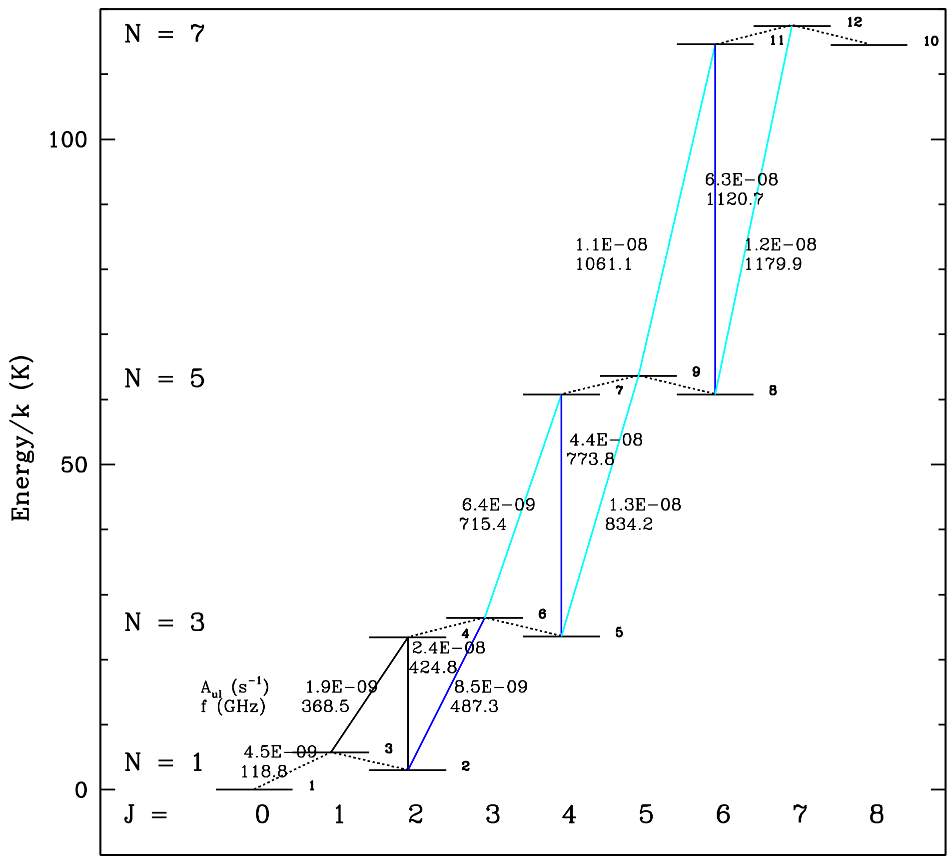

Figure 1. Lower rotational energy levels and transitions of O_2 molecule. Each level is denoted by its rotational quantum number, N, and total angular momentum quantum number, J. Only odd values of N are allowed due to the homonuclear nature of the oxygen molecule, and the transitions are all magnetic dipole transitions. For each, we give the frequency in GHz and above that, the spontaneous decay rate in s^{-1}.

2. Data reduction procedure.

The HOP data were downloaded from the Herschel Science Archive and reprocessed with the standard HIFI pipeline to level 2.0, using HIPE 8.0 (build 3449). Level 2 data were then exported to the FITS format using the HIPE task `hiClass()` and the subsequent data processing was carried out using the IRAM CLASS software package (https://www.iram.fr/IRAMFR/GILDAS/). The spectra were visually inspected to identify spurs that were not automatically flagged by the pipeline. The affected channels were blanked and excluded from the subsequent analysis. Individual local oscillator (LO) settings for a given source were combined into a single CLASS files (located in the `dsb` folder). The file names correspond to the Herschel OBSIDs and a list of all observations is included below. The cleaned double-sideband (DSB) spectra were deconvolved in CLASS to produce the equivalent single-sideband (SSB) spectra. The deconvolution algorithm is the same as that used in the HIPE `doDeconvolution()` task and the resulting spectra are located in the `ssb` folder.

The deconvolution algorithm has been design to work with a set of spectra covering a wide range of frequencies in multiple LO settings, rather than several closely spaced frequency settings used in HOP. The deconvolved spectra should thus be used only as a guide for the upper/lower sideband line identification. Any spectral features that may be present should be independently verified in the individual DSB spectra. Observation 1342216354 (OMC-1 Peak 1) had a different pointing and therefore line and continuum intensities from observations 1342203744–1342203751. Therefore the two data sets cannot be combined for the deconvolution. Observation 1342191684 (Sgr B2S) contains no lines and cannot be deconvolved; only the DSB spectra are provided.

Line temperatures of the DSB and SSB spectra have *not* been corrected for the Herschel beam efficiency. The latest beam efficiency values can be found in Roelfsema et al. (2012; A&A, 537, A17).

For the maps of rho Oph (observations 1342228583–1342228590), spectra obtained with different LO settings are not deconvolved, but simply averaged, aligned with respect to the signal sideband frequency. Lines from image sideband thus appear as multiple features in the averaged spectra. The `*bas` files in the folder `maps_dsb` contain baseline subtracted DSB spectra for the 8 individual maps. Different backends are written as separate scans. The CLASS file `1342228583-1342228590.hifi` contains spectra at the four positions, labeled O1–O4 in Liseau et al. (2012), convolved to the 43.8" HIFI beam at 487 GHz. Different maps and spectrometers are written as separate scans. The file `1342228583-1342228590_a.hifi` contains final averaged spectra from all maps. The H and V polarizations are written out separately, than averaged together. The HRS and WBS spectra are written as separate scans.

Final reduced spectra were exported to the CLASS FITS format and subsequently reprocessed in HIPE to produce FITS files readable by HIPE and other FITS viewers. The final FITS files for this data release can be found in the folders `dsb_hipe`, `ssb_hipe`, and `maps_hipe`.

The CLASS scripts used in the data reduction can be found in the `class` folder and the HIPE scripts used for reprocessing the FITS files can be found in the `hipe` folder.

4. List of HOP data products.

Individual LOs

OD	Obs. Id	Target	Transition
406	1342199079	AFGL 2591	487.3GHz
406	1342199080	AFGL 2591	487.3GHz
406	1342199081	AFGL 2591	487.3GHz
406	1342199082	AFGL 2591	487.3GHz

406	1342199083	AFGL 2591	487.3GHz
406	1342199084	AFGL 2591	487.3GHz
406	1342199085	AFGL 2591	487.3GHz
406	1342199086	AFGL 2591	487.3GHz
561	1342210155	AFGL 2591	773.8GHz
561	1342210156	AFGL 2591	773.8GHz
561	1342210157	AFGL 2591	773.8GHz
561	1342210158	AFGL 2591	773.8GHz
561	1342210159	AFGL 2591	773.8GHz
561	1342210160	AFGL 2591	773.8GHz
561	1342210161	AFGL 2591	773.8GHz
561	1342210162	AFGL 2591	773.8GHz
561	1342210144	AFGL 2591	1120.7GHz
561	1342210145	AFGL 2591	1120.7GHz
561	1342210146	AFGL 2591	1120.7GHz
561	1342210147	AFGL 2591	1120.7GHz
561	1342210148	AFGL 2591	1120.7GHz
561	1342210149	AFGL 2591	1120.7GHz
561	1342210150	AFGL 2591	1120.7GHz
561	1342210151	AFGL 2591	1120.7GHz
445	1342202025	NGC 1333 IRAS 4A	487.3GHz
445	1342202026	NGC 1333 IRAS 4A	487.3GHz
445	1342202027	NGC 1333 IRAS 4A	487.3GHz
445	1342202028	NGC 1333 IRAS 4A	487.3GHz
445	1342202029	NGC 1333 IRAS 4A	487.3GHz
445	1342202030	NGC 1333 IRAS 4A	487.3GHz
445	1342202031	NGC 1333 IRAS 4A	487.3GHz
445	1342202032	NGC 1333 IRAS 4A	487.3GHz
474	1342203744	OMC-1 (Peak 1)	487.3GHz
474	1342203745	OMC-1 (Peak 1)	487.3GHz
474	1342203746	OMC-1 (Peak 1)	487.3GHz
474	1342203747	OMC-1 (Peak 1)	487.3GHz
474	1342203748	OMC-1 (Peak 1)	487.3GHz
474	1342203749	OMC-1 (Peak 1)	487.3GHz
474	1342203750	OMC-1 (Peak 1)	487.3GHz
474	1342203751	OMC-1 (Peak 1)	487.3GHz
673	1342216354	OMC-1 (Peak 1)	487.3GHz
504	1342205340	OMC-1 (Peak 1)	773.8GHz

504	1342205341	OMC-1 (Peak 1)	773.8GHz
504	1342205342	OMC-1 (Peak 1)	773.8GHz
504	1342205343	OMC-1 (Peak 1)	773.8GHz
504	1342205344	OMC-1 (Peak 1)	773.8GHz
504	1342205345	OMC-1 (Peak 1)	773.8GHz
504	1342205346	OMC-1 (Peak 1)	773.8GHz
504	1342205347	OMC-1 (Peak 1)	773.8GHz
505	1342206129	OMC-1 (Peak 1)	1120.7GHz
505	1342206130	OMC-1 (Peak 1)	1120.7GHz
505	1342206131	OMC-1 (Peak 1)	1120.7GHz
505	1342206132	OMC-1 (Peak 1)	1120.7GHz
505	1342206133	OMC-1 (Peak 1)	1120.7GHz
505	1342206134	OMC-1 (Peak 1)	1120.7GHz
505	1342206135	OMC-1 (Peak 1)	1120.7GHz
505	1342206136	OMC-1 (Peak 1)	1120.7GHz
503	1342205284	Sgr A (50 km/s)	487.3GHz
503	1342205285	Sgr A (50 km/s)	487.3GHz
503	1342205286	Sgr A (50 km/s)	487.3GHz
503	1342205287	Sgr A (50 km/s)	487.3GHz
503	1342205288	Sgr A (50 km/s)	487.3GHz
503	1342205289	Sgr A (50 km/s)	487.3GHz
503	1342205290	Sgr A (50 km/s)	487.3GHz
503	1342205291	Sgr A (50 km/s)	487.3GHz
491	1342204804	Sgr A (50 km/s)	773.8GHz
491	1342204805	Sgr A (50 km/s)	773.8GHz
491	1342204806	Sgr A (50 km/s)	773.8GHz
491	1342204807	Sgr A (50 km/s)	773.8GHz
491	1342204808	Sgr A (50 km/s)	773.8GHz
491	1342204809	Sgr A (50 km/s)	773.8GHz
491	1342204810	Sgr A (50 km/s)	773.8GHz
491	1342204811	Sgr A (50 km/s)	773.8GHz
509	1342205836	Orion Bar	773.8GHz
509	1342205837	Orion Bar	773.8GHz
509	1342205838	Orion Bar	773.8GHz
509	1342205839	Orion Bar	773.8GHz
509	1342205840	Orion Bar	773.8GHz
509	1342205841	Orion Bar	773.8GHz
509	1342205842	Orion Bar	773.8GHz
509	1342205843	Orion Bar	773.8GHz

681	1342216822	NGC 6334I	487.3GHz
681	1342216823	NGC 6334I	487.3GHz
681	1342216824	NGC 6334I	487.3GHz
681	1342216825	NGC 6334I	487.3GHz
681	1342216826	NGC 6334I	487.3GHz
681	1342216827	NGC 6334I	487.3GHz
681	1342216828	NGC 6334I	487.3GHz
681	1342216829	NGC 6334I	487.3GHz
667	1342215940	NGC 6334I	773.8GHz
667	1342215941	NGC 6334I	773.8GHz
667	1342215942	NGC 6334I	773.8GHz
667	1342215943	NGC 6334I	773.8GHz
667	1342215944	NGC 6334I	773.8GHz
667	1342215945	NGC 6334I	773.8GHz
667	1342215946	NGC 6334I	773.8GHz
667	1342215947	NGC 6334I	773.8GHz
672	1342216319	rho Oph A (P2)	487.3GHz
672	1342216320	rho Oph A (P2)	487.3GHz
672	1342216321	rho Oph A (P2)	487.3GHz
672	1342216322	rho Oph A (P2)	487.3GHz
672	1342216323	rho Oph A (P2)	487.3GHz
672	1342216324	rho Oph A (P2)	487.3GHz
672	1342216325	rho Oph A (P2)	487.3GHz
672	1342216326	rho Oph A (P2)	487.3GHz
672	1342216311	rho Oph A (P3)	487.3GHz
672	1342216312	rho Oph A (P3)	487.3GHz
672	1342216313	rho Oph A (P3)	487.3GHz
672	1342216314	rho Oph A (P3)	487.3GHz
672	1342216315	rho Oph A (P3)	487.3GHz
672	1342216316	rho Oph A (P3)	487.3GHz
672	1342216317	rho Oph A (P3)	487.3GHz
672	1342216318	rho Oph A (P3)	487.3GHz
673	1342216346	rho Oph A (H2O)	487.3GHz
673	1342216347	rho Oph A (H2O)	487.3GHz
673	1342216348	rho Oph A (H2O)	487.3GHz
673	1342216349	rho Oph A (H2O)	487.3GHz
673	1342216350	rho Oph A (H2O)	487.3GHz
673	1342216351	rho Oph A (H2O)	487.3GHz

673	1342216352	rho Oph A (H2O)	487.3GHz
673	1342216353	rho Oph A (H2O)	487.3GHz

Spectral Scans

OD	Obs. Id	Target	Transition
291	1342191483	Sgr B2 (S)	487.3GHz
291	1342191503	OMC-1 (Peak 1)	487.3GHz
291	1342191506	Orion Bar	487.3GHz
292	1342191557	rho Oph A	487.3GHz
295	1342191684	Sgr B2 (S)	1120.7GHz
297	1342191739	rho Oph A	773.8GHz
297	1342191740	Sgr B2 (S)	773.8GHz
297	1342191753	Orion Bar	773.8GHz
297	1342191754	OMC-1 (Peak 1)	773.8GHz
309	1342192336	AFGL 2591	773.8GHz
310	1342192359	AFGL 2591	487.3GHz

Maps

OD	Obs. Id	Target	Transition
853	1342228583	rhoOph(p2p3h2o)	773.8GHz
853	1342228584	rhoOph(p2p3h2o)	773.8GHz
853	1342228585	rhoOph(p2p3h2o)	773.8GHz
853	1342228586	rhoOph(p2p3h2o)	773.8GHz
853	1342228587	rhoOph(p2p3h2o)	773.8GHz
853	1342228588	rhoOph(p2p3h2o)	773.8GHz
853	1342228589	rhoOph(p2p3h2o)	773.8GHz
853	1342228590	rhoOph(p2p3h2o)	773.8GHz

5. Follow up information and references

The publications involving HOP data published to date are given below. Additional data reduction and analysis is still in progress. The paper by Goldsmith et al. (2011) has an extensive bibliography of previous searches for molecular oxygen in the interstellar medium.

Goldsmith, P.F., Liseau, R., Bell, T.A., et al., *Herschel* Measurements of Molecular Oxygen in Orion, 2011, Ap.J., 737, 96

Liseau, R., Goldsmith, P.F., Larsson, B., et al., "Multi-Line Detection of O_2 towards ρ Ophiuchi A, 2012, A&A, 541, A73

Melnick, G.J., Tolls, V., Goldsmith, P.F. et al. "*Herschel* Search for O_2 Toward the Orion Bar", 2012, ApJ, 752, 26